Ultrathin Bifacial Passivated Emitter and Rear Cell with Inverted Pyramid Textures

Chengjing Shi, Yuan Fan, Yuhua Gu, Borong Sang, Sihua Zhong, Xiangyang Kong, Wenzhong Shen, Xiaomin Song,* and Zengguang Huang*

Wafer thinning is a crucial technique for high-efficiency solar cells. Herein, an inverted pyramid (IP) texture is prepared on a 35 µm-thick flexible silicon (Si) wafer with a standard area of 156 × 156 mm². Based on the experimental results, an ultrathin bifacial passivated emitter and rear cell (PERC) with IP textures using PC1D simulation is designed. The influence of wafer thickness, IP texture, bifacial structure, thickness of the antireflection coating, and doping concentration on device performance is investigated. The results show that the ultrathin IP-based bifacial PERC possesses better output performance than the traditional cell. Finally, a simulated maximum efficiency of 23.44% is obtained using PC1D software, with an open-circuit voltage of 0.7127 V and a short-circuit current of 9.272 A. This ultrathin PERC with IP textures provides an effective way to improve the efficiency of ultrathin silicon solar cells.

1. Introduction

Ultrathin silicon (Si) solar cells have attracted much research interest because of their reduced usage of Si materials, good flexibility, and wearability.[1–3] They demonstrate great potential for expanding the application of high-efficiency silicon solar cells. However, as the thickness of the silicon bulk decreases, the light absorption is significantly reduced.[4,5] As a result, it is necessary

C. Shi, Y. Fan, Y. Gu, S. Zhong, X. Song, Z. Huang
School of Science, and School of Chemical Engineering
Jiangsu Ocean University
Lianyungang 222005, Jiangsu Province, P. R. China
E-mail: xmsong@jou.edu.cn; zghuang@jou.edu.cn

B. Sang
School of Photovoltaic and Renewable Energy Engineering
UNSW
Sydney 2052, Australia

Z. Huang
Jiangsu Institute of Marine Resources Development
Lianyungang 222005, Jiangsu Province, P. R. China

X. Kong, W. Shen
School of Physics and Astronomy
School of Materials Science and Engineering
Key Laboratory of Artificial Structures and Quantum Control (Ministry of Education)
Shanghai Jiao Tong University
Shanghai 200240, P. R. China

The ORCID identification number(s) for the author(s) of this article can be found under https://doi.org/10.1002/pssa.202100481.

to develop new texturing techniques to provide a superior light-trapping effect and suppress optical losses in the devices. Yu et al.[6] developed a cutting technology for silicon wafers with a thickness of less than 100 µm, guiding the preparation of ultrathin silicon wafers. Wang et al.[7] introduced an inverted pyramid (IP) structure and fabricated a passivated emitter local back diffusion monosilicon solar cell on a 47 µm-thick silicon wafer with an efficiency (η) of 21.5%. Tang et al.[8] developed 45 µm-thick ultrathin silicon wafers by copper-assisted chemical thinning and fabricated a crystalline silicon solar cell with an η of 17.3% by designing an asymmetric surface texture on the front and back. Branham et al.[9] prepared periodic nanostructures on the surface of 10 µm crystalline silicon and optimized the etching process to obtain a solar cell η of 15.7%. Petermann et al.[10] used a porous silicon layer transfer technology to prepare a crystalline silicon solar cell with a thickness of 43 µm and an η of 19%. Do et al.[11] prepared a thin monocrystalline silicon wafer with a thickness of 100 µm using an alkali etching thinning treatment, and their η reached 16.8% on a solar cell with a size of 156 × 156 mm².

Suppressing the front-surface residual reflection, ensuring excellent rear passivation, and improving the rear light absorption are effective ways to improve the performance of ultrathin solar cells. To this end, nanostructures[12–14] and IP structures[15,16] are suitable for ultrathin solar cells because of their better light-trapping ability than the upright pyramid (UP). Passivated emitter and rear cell (PERC) structures[17,18] have also proven to be an effective way to achieve rear passivation. Additionally, because the propagation path of the incident light becomes shorter in the thinner silicon wafers, some of the photons pass through the wafer. Therefore, bifacial PERC with IP textures can simultaneously improve the light-trapping performance of the front surface, rear passivation, and optical gain through additional light absorption at the rear.

In this study, front IP textures and rear passivated structures were applied to ultrathin bifacial solar cells. First, we prepared a flexible 35 µm-thick wafer with an area of 156 × 156 mm² and introduced the IP textures using the metal-assisted chemical etching (MACE) technique. Then, we systematically investigated the influence of wafer thickness, IP textured surface, bifacial structure, antireflection coating, and doping concentration on

the performance of the ultrathin bifacial PERC using PC1D simulation software (Version 5.9). Based on the optimization of simulated parameters, we numerically obtained a high-performance output for the ultrathin PERC with IP textures, demonstrating a promising prospect for high-efficiency Si solar cells.

2. IP Preparation and Optical Performance

As shown in **Figure 1**a, a 35 μm-thick silicon wafer can be bent completely for use in a flexible device. However, the thinning of silicon wafers also limits the absorption of light in the silicon bulk, and, therefore, the development of an alternative textured surface with better light-trapping performance is of great importance for improving the performance of ultrathin devices. The IP structure of silicon increases the light absorption of the solar cell owing to its superior light-trapping performance compared to the traditional UP, especially in the short-wavelength range.[19–21] Additionally, its low surface ratio does not lead to severe surface recombination. Consequently, the short-circuit current (I_{sc}) and open-circuit voltage (V_{oc}) of the ultrathin solar cells can be simultaneously improved, resulting in a higher η for the device.

To make the ultrathin IP textured wafer, traditional alkaline solution etching was first used to prepare ultrathin silicon wafers with a thickness of 35 μm. Then, a simple, low-cost, and compatible MACE method combined with alkaline anisotropic etching was applied to create the IP structure on the surface. We used 156×156 mm^2 (pseudosquare) solar grade Cz p-type (100)

wafers with a thickness of 180 ± 10 μm and a resistivity of ≈ 3 Ω cm. The preparation process was as follows: a wafer was first cleaned via a standard RCA cleaning process. Then, the silicon wafer was immersed in a 10 wt% NaOH solution at a temperature of 75 °C for an etching time of 100 min to obtain an ultrathin wafer. The wafer was then put into a solution of HF(2 M)/AgNO$_3$(0.0005 M)/H$_2$O$_2$(1.06 M), and the MACE method was used to etch a nanoporous silicon structure on its surface for 6 min. Afterward, the residual silver was removed by an HNO$_3$ solution to obtain a porous silicon surface. Next, the wafer was etched in a mixed acid solution of HF/HNO$_3$ = 1:3 (vol) at 6–9 °C for 90 s to remove the layer of porous silicon on the surface and achieve nanoholes for the nanoporous structure at the bottom. Finally, to obtain a uniform IP structure, the silicon wafer with nanoholes was transferred into an NaOH (1%) solution with additives at 80 °C and anisotropic etching was performed.

Figure 1b shows photographs of the Si wafers with UP and IP textures. We can see that the IP sample is visually darker than the UP sample, which means that the IP sample has better light-trapping performance. Samples of the IP and UP surfaces were also treated with a plasma-enhanced chemical vapor deposition SiO$_x$ (≈ 2 nm)/SiN$_x$ (≈ 75 nm) antireflection coating. The measured reflectance of the coated samples in the 350–1100 nm wavelength range, as shown in Figure 1e, also confirmed the greater light-trapping ability of the IP structure. Notably, the reflectance of the IP with SiO$_x$/SiN$_x$ is lower than that of UP with SiO$_x$/SiN$_x$ over a broad wavelength range, indicating the optical superiority of IP-based solar cells compared to UP-based ones.
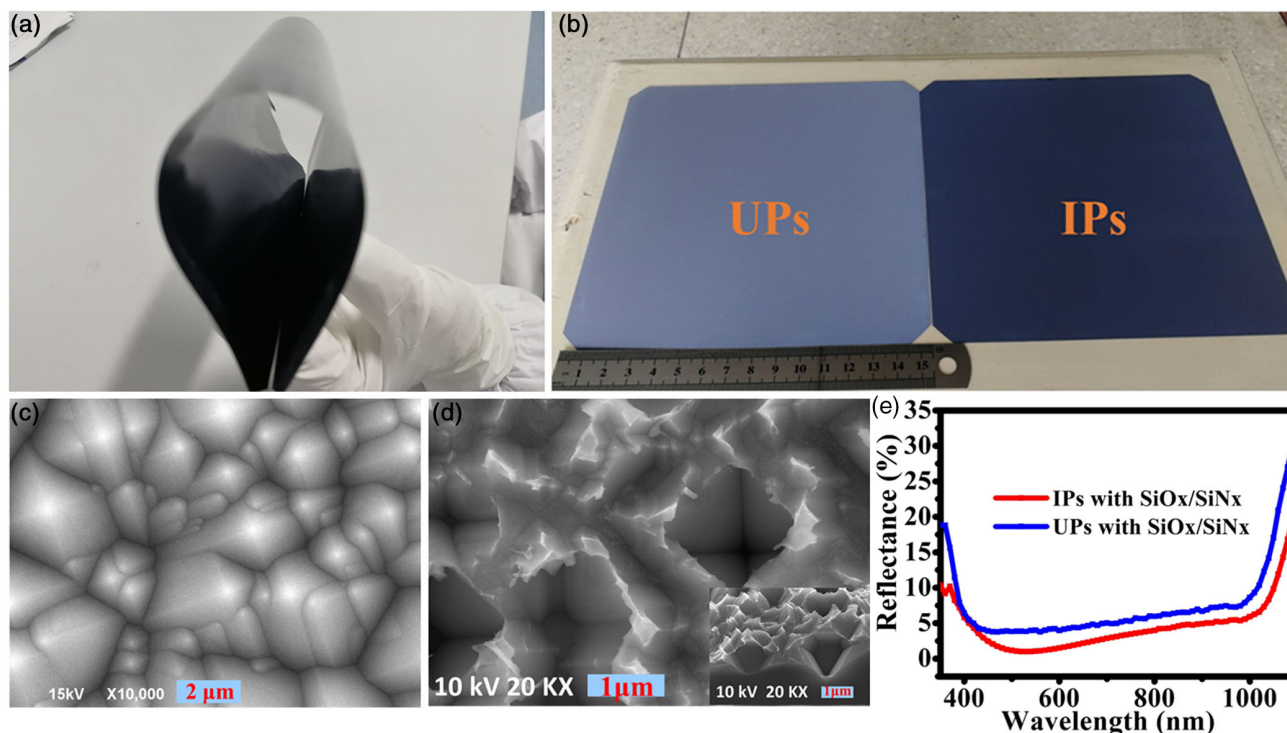

Figure 1. a) Ultrathin flexible wafer with a thickness of 35 μm. b) Appearance comparison between IP and UP textured surface. c) Scanning electron microscopy (SEM) image of UP textured surface. d) SEM image of IP textured surface (cross section in inset). e) Reflectance of IP and UP samples with SiO$_x$/SiN$_x$ antireflection coatings.

ADVANCED SCIENCE NEWS
www.advancedsciencenews.com

pss a
physica status solidi a
www.pss-a.com

In addition, the calculated solar averaged reflectance, R_{ave}, over the AM1.5 spectrum in the wavelength range of 350–1100 nm is much lower for the IP with SiO_x/SiN_x sample (3.8%) than for the UP with SiO_x/SiN_x sample (6.4%). The microstructures observed via SEM of the two structures are shown in Figure 1c,d. The feature size of the IP structure is in the range of 800–1000 nm, whereas the size of the UP structure is approximately 3 μm. With all of these advantages, it is foreseeable that the optical performance of a device using the IP texture will be improved, which will, in turn, improve the I_{sc} and η of the device.

3. Results and Discussion

3.1. PC1D Modeling

The device structure of the bifacial PERC solar cells with IP textures is shown in **Figure 2**. The designed device combines the front submicrometer IP array and rear passivation, making full use of the excellent frontal antireflection, good rear internal reflection, and ultralow rear-surface recombination. This device is expected to achieve an excellent broadband spectral response by improving the optical and electrical performances of both the front and back surfaces. In this study, we used a dual-diode model for the bifacial PERC solar cells using a PC1D simulation. The simulation parameters were set with reference to the current PERC manufacturing techniques, but it is necessary to point out that our parameters were beyond those currently achievable at an industrial level. Although some parameters cannot be reached on the production line at present, they may be viable in a few years. Using these parameters ensures the future reliability and applicability of the simulation results and provides direction for manufacturing improvements. The detailed parameter settings are listed in **Table 1**.

Note that, first, PC1D with version 5.9 is based on the Boltzmann statistics and there is the degeneracy effects in heavily doped region.[22,23] Second, neglecting the impurity band from the aluminum doped back-surface field leads to a deviation of simulative result because of the limit of the modeling with the intrinsic density-of-states. Third, incomplete ionization of dopants in moderately doped surface regions results in a
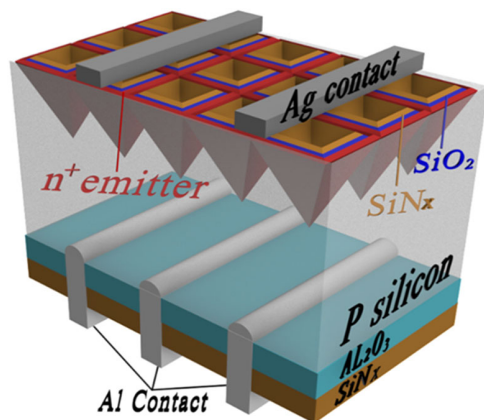
Table 1. PC1D parameters setting for p-type bifacial PERC with IP.

Parameters		Value
Device area		244.33 cm²
Angle of IP		−54.74°
Depth of IP		1 μm
Front-surface SiO_2		2 nm
Front-surface SiN_x		74.27 nm
Rear-surface Al_2O_3		2 nm
Rear-surface SiN_x		75 nm
Device thickness		175 nm
Emitter doping level		$3 \times 10^{17}\ cm^{-3}$
Front diffusion depth		0.3 μm
Rear doping level		$6 \times 10^{16}\ cm^{-3}$
Rear diffusion depth		4 μm
Bulk recombination		650 μs
Front-surface recombination		100 cm s⁻¹ (monofacial) 100 cm s⁻¹ (bifacial)
Rear-surface recombination		550 cm s⁻¹ (monofacial) 550 cm s⁻¹ (bifacial)
Internal reflection	IP	65% (R_{f1}) 82% (R_{f2}) 65% (R_{b1}) 65% (R_{b2})
	UP	77% (R_{f1}) 96% (R_{f2}) 76% (R_{b1}) 76% (R_{b2})

deviation in in the simulated recombination current density and sheet resistance.[24]

In this article, the modeling implies the following input assumptions: 1) The ideal solar cell is based on two-diode model. The first and second saturation current density are set as 3×10^{-12} and 2×10^{-8} A cm⁻², respectively. 2) The bulk lifetime of p-type monocrystalline Si substrate is set as 650 μs. 3) The parameters of internal reflection are determined by the external reflections and absorptions from Wafer Ray Tracer. 4) For the bifacial case, the secondary light source is enabled and the intensity of illumination is set as the 4% of 1 Sun.

3.2. Thickness Dependence

One of the primary influences on the performance of ultrathin solar cells is the cell thickness. As shown in **Figure 3**a, when the cell thickness is reduced from 175 to 35 μm, the external quantum efficiency (EQE) of the cells remained at the same level in the wavelength range of 300–700 nm. This means that the incident light in the short and medium wavelength ranges can be completely absorbed at a shallow depth on the surface of the solar cell. However, the decrease in cell thickness causes a reduction of the EQE in the wavelength range of 700–1200 nm. When the thickness of the device is smaller than 70 μm, the decrease in EQE becomes more serious, which is attributed to the sharp decline of light absorption in the thinner silicon wafer.

We also studied the influence of the device thickness on I_{sc} and η for the cell thickness ranging from 20 to 175 μm, as shown in Figure 3b. It can be seen that as the thickness of the cell is

Figure 2. Schematic diagram of the simulated solar cell structure.

ADVANCED
SCIENCE NEWS
www.advancedsciencenews.com

physica
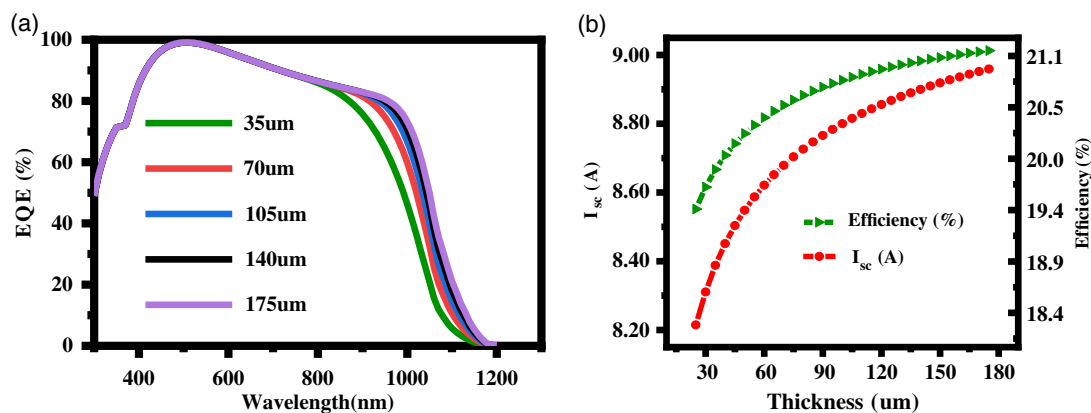pss status solidi a
www.pss-a.com

Figure 3. a) EQE of devices of different thickness. b) Short-circuit current (I_{sc}) and efficiency versus cell thickness.

reduced from 175 to 20 μm, I_{sc} is reduced from 8.96 to 8.21 A, and η falls from 21.12% to 19.45%. This is consistent with the mechanism shown in Figure 3a. As an indirect bandgap material, silicon has a relatively low absorption coefficient. For short-wavelength bands, the absorption depth is shallow and can be absorbed entirely around the emitter. The absorption depth for long-wavelength bands is deeper; when the cell thickness decreases, the absorption decreases, resulting in a decrease in I_{sc}. Moreover, as the cell was further thinned, the slope of the I_{sc} curve gradually increased, meaning that the thinner the silicon chip, the lower the absorption rate of medium- and long-wavelength photons. Meanwhile, the V_{oc} remained unchanged as the solar cell thickness reduced to 20 μm. According to the above results, I_{sc} and η are correlated with the thickness of the cell, while V_{oc} is not. It can be concluded that the decrease in I_{sc} is the primary cause of the decrease in η.

3.3. IP Textures and Bifacial Structures

Advanced light-trapping structures are an effective way to improve the performance of ultrathin solar cells. Compared with the UP widely used in the industry, the IP surface has better light-trapping performance because it causes incident light in the structure to reflect multiple times. Based on the analysis in Section 3.2, we set the thickness of the wafer to 35 μm, which is 1/5 of the standard thickness of 175 μm, to determine the influence of the IP textured surface on the performance of ultrathin PERC solar cells. The device performance parameters of the solar cell with the traditional UP texture (size of 1 μm) and the solar cell with the IP structures (1 μm) are shown in **Table 2**. It was found that both devices maintained the same V_{oc}, but I_{sc} increased by 137 mA with the IP structure. This is because

the IP structure reflects incident light more times than the UP structure and thus shows better light-trapping performance. Owing to the increase in I_{sc}, we ultimately achieved an increase in η of 0.34% for the solar cell with the IP structure.

As the thickness of the silicon wafer decreases, more long-wavelength photons pass through it, which causes inefficient light utilization in the cells. Therefore, it is desirable to adopt a bifacial structure to further increase the total incident light absorption.[25,26] Compared with the monofacial solar cell, a bifacial structure can collect an extra 6–10% of the incident light that would otherwise be lost, thereby increasing the power generation of the device. The output performance comparison of the monofacial and bifacial devices is presented in Table 2. Compared with the output parameters of monofacial solar cells, the I_{sc} of the bifacial solar cell is increased by 55 mA, and the η is increased by 0.62%. This reveals that the bifacial structure is superior to the monofacial structure.

3.4. Parameter Optimization of Ultrathin IP-Based Bifacial PERC

The doping concentration of the emitter determines the value of the built-in potential, which is closely related to the output of the solar cell.[27] A proper doping concentration is conducive to forming ohmic contacts, reducing the series resistance, and improving the η of the device. At the same time, doping concentrations that are too low or too high will decrease the I_{sc} of the device and increase recombination. Therefore, it is necessary to explore the optimal doping concentration in the emitter of the ultrathin bifacial PERC through simulations.

We set the range of emitter doping concentrations to 6×10^{16}–6×10^{19} cm^{-3}. As shown in **Figure 4**a, as the emitter doping concentration increased, the V_{oc} first increased and then decreased, reaching its maximum value of 0.6839 V when the concentration was 3×10^{18} cm^{-3}. The main reason for this peak is that when the emitter doping concentration is low, the conductivity of the emitter region is low. Thus, the internal series resistance increases, resulting in a low filled factor (FF). However, when the doping concentration increases, the conductivity of the n-type region is greatly improved, and the barrier height of the p–n junction is also extended, resulting in an increase in V_{oc} and FF. When the doping concentration exceeds 3×10^{18} cm^{-3}, there
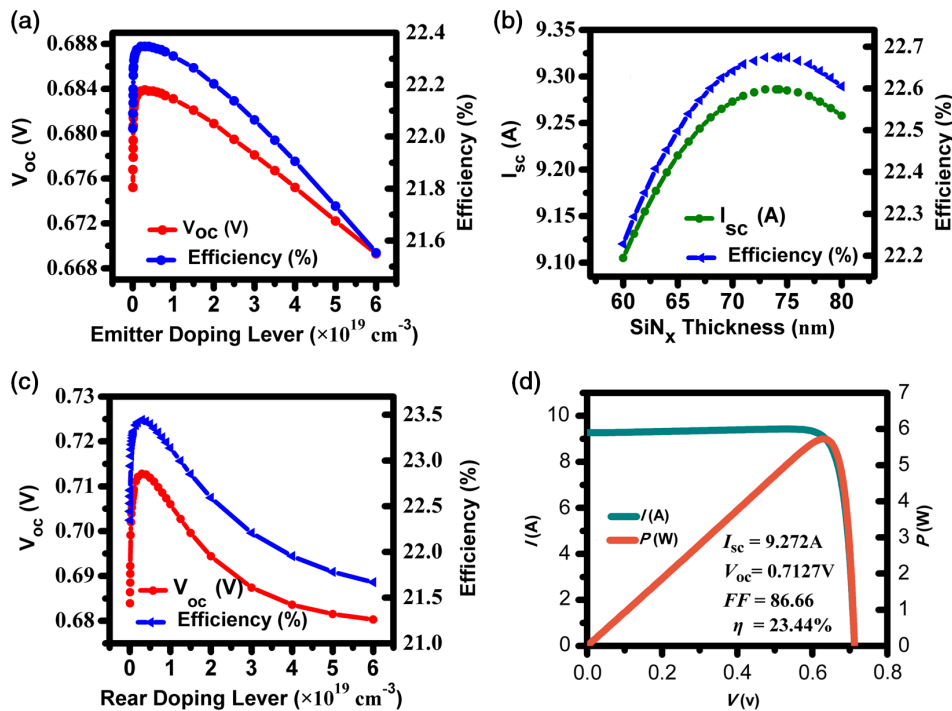
Table 2. Comparison of output performances between monofacial and bifacial solar cells.

Cell type	I_{sc} [A]	V_{oc} [V]	η [%]
Monofacial with UP	9.057	0.6857	21.44
Monofacial with IP	9.194	0.6861	21.78
Bifacial with IP	9.249	0.6861	22.40

**ADVANCED
SCIENCE NEWS**
www.advancedsciencenews.com

**physica
pss status solidi a**
www.pss-a.com

Figure 4. a) Influence of emitter doping concentration on V_{oc} and η in different thickness. b) Influence of SiN$_x$ thickness on V_{oc} and η. c) Rear doping concentration as a function of V_{oc} and η. d) The I–V and P–V results of optimized bifacial IP PERC.

is a heavy doping effect that causes a narrower forbidden band-width and a much higher Auger recombination, rapidly decreasing the V_{oc} of the device. Moreover, as shown in **Table 3**, I_{sc} exhibits a downward trend as the emitter doping concentration increases because a higher doping concentration reduces the minority carrier diffusion length and resistivity. Based on the above analysis, the η of the cell initially increased and then decreased with an increase in the emitter doping concentration. When the doping concentration reaches 3×10^{18} cm^{-3}, the η of the solar cell reaches a peak value of 22.35%.

We also optimized the thickness of the SiO$_2$/SiN$_x$ laminated antireflection coating with the IP structure to further reduce the

optical losses. The thickness of the ultrathin SiO$_2$ passivation layer was set to a fixed value of 2 nm. As shown in Figure 4b, when the thickness of SiN$_x$ increased from 60 to 80 nm, I_{sc} increased and then decreased, reaching a maximum value of 9.286 A at 74.27 nm. Thus, the optimal IP solar cell structure includes a 2 nm-thick SiO$_2$ layer and a 74.27 nm-thick SiN$_x$ layer, which produces the best destructive interference effect on the incident light. The absolute increase of η was 0.44% over the simulated range, and the absolute decrease was 0.07%. Ignoring the slight influence of V_{oc} on η, we found that the gain and loss of η can be mainly attributed to the change in I_{sc} from the different thicknesses of the SiO$_2$/SiN$_x$ coatings.

Finally, we studied the effect of rear doping on device performance. According to Figure 4c, as the rear doping concentration increases from 1×10^{16} to 2.9×10^{18} cm^{-3}, the V_{oc} increases by 29 mV, reaching a maximum value of 0.7127 V. The doping concentration at the rear contact in a solar cell has a significant impact on its electrical performance. This is because the back acceptor doping forms a p–p$^+$ junction, and the direction of the built-in electric field is consistent with the polarity of the pho-togenerated voltage, which effectively reduces the minority carrier recombination and enlarges the total built-in potential difference. When the doping concentration continues to increase, V_{oc} gradually decreases to 0.680 V. This is because the diffusion length of minority carriers is much longer than the thickness of the device. Moreover, excessively high doping processes, such as thermal diffusion, ion implantation, and laser doping, introduce many impurities and crystal defects, causing severe Auger recombination in the p$^+$ region. This is the reason for the sharp drop in V_{oc} and η. I_{sc} shows a downward trend with

Table 3. Output performance dependence on emitter doping concentration, rear doping concentration, and SiN$_x$ thickness.

Parameter	Value	Output		
		V_{oc} [V]	I_{sc} [A]	η [%]
Emitter doping level	6×10^{16} cm^{-3}	0.675	9.267	22.03
	3×10^{18} cm^{-3}	0.684	9.266	22.35
	6×10^{19} cm^{-3}	0.669	9.153	21.55
SiN$_x$ thickness	60 nm	0.691	9.105	22.23
	74.27 nm	0.691	9.286	22.67
	80 nm	0.691	9.258	22.60
Rear doping level	6×10^{16} cm^{-3}	0.684	9.266	22.35
	2.9×10^{18} cm^{-3}	0.713	9.272	23.44
	6×10^{19} cm^{-3}	0.680	9.086	21.67

increasing rear doping concentration, as shown in Table 3. Based on Figure 4c and Table 3, it was concluded that the V_{oc} and η of the solar cell are positively correlated with the change in the rear doping concentration.

When all the optimal parameters were set in the ultrathin PERC with IP textures, PC1D modeling predicted that the maximum η can reach up to 23.44%, with a V_{oc} of 0.7127 V and the I_{sc} of 9.272 A. Figure 4d shows the optimal I–V and P–V curves of the device. Based on the above discussions, we determined that in the case of bifacial cell structures, the IP texture and low doping concentration of the emitter and back side are the keys to the success of the ultrathin solar cell.

4. Conclusions

In this work, IP structures were fabricated on an ultrathin (35 μm) 156×156 mm^2 standard solar-grade silicon wafer, and the measured reflectance of the IP texture with SiO_x/SiN_x coatings indicated that the IP structure has a better light-trapping effect than the UP structure. Based on these experimental results, we designed a p-type flexible ultrathin IP-based bifacial PERC model utilizing PC1D software. By investigating the effects of cell thickness, IP structure, bifacial structure, antireflection coating thickness, emitter doping concentration, and rear doping concentration on the performance of the solar cell, we obtained the optimized device parameters: the SiN_x thickness was 74.27 nm, the emitter doping concentration was 3×10^{18} cm^{-3}, and the rear doping concentration was 2.9×10^{18} cm^{-3} for the optimized cell. Benefiting from the optimization of the optical and electrical parameters, a maximum η of 23.44% on a 35 μm-thick ultrathin IP-based bifacial PERC solar cell was numerically obtained by PC1D simulation. The proposed solar cell shows a significantly higher output performance than traditional solar cells. The superior flexibility, material saving, high performance, and production-line compatibility make this novel photovoltaic device a promising prospect for mass production of high-performance solar cells.

Conflict of Interest

The authors declare no conflict of interest.

Data Availability Statement

Research data are not shared.

[1] A. W. Blakers, T. Armour, Sol. Energy Mater. Sol. Cells 2009, 93, 1440.

[2] G. P. Willeke, Sol. Energy Mater. Sol. Cells 2002, 72, 191.

[3] M. M. Wang, Data of Master's Thesis, Nanjing University of Aeronautics and Astronautics, 2019.

[4] Y. Li, S. Zhong, Y. Zhuang, L. Yang, F. Meng, W. Wang, Z. Li, W. Shen, Adv. Electron. Mater. 2019, 5, 14.

[5] F. Ye, N. Yuan, J. Ding, Z. Feng, J. Renew. Sustain. Energy 2015, 7, 1.

[6] X. Yu, P. Wang, X. Li, D. Yang, Sol. Energy Mater. Sol. Cells 2012, 98, 337.

[7] A. Wang, J. Zhao, S. R. Wenham, M. A. Green, Progr. Photovolt. Res. Appl. 1996, 4, 55.

[8] Q. Tang, H. Shen, H. Yao, K. Gao, Y. Jiang, W. Yang, Y. Liu, Sol. Energy 2018, 170, 263.

[9] M. S. Branham, W. Hsu, S. Yerci, J. Loomis, S. V. Boriskina, B. R. Hoard, S. E. Han, G. Chen, Adv. Mater. 2015, 27, 2182.

[10] J. H. Petermann, D. Zielke, J. Schmidt, F. Haase, E. G. Rojas, R. Brendel, Progr. Photovolt. Res. Appl. 2011, 20, 1.

[11] K. S. Do, T. H. Baek, M. G. Kang, S. J. Choi, G. H. Kang, G. J. Yu, J. C. Lee, J.-M. Myoung, H.-E. Song, Metals Mater. Int. 2014, 20, 545.

[12] F. Sobhani, H. Heidarzadeh, H. Bahador, Opt. Quant. Electron. 2020, 52, 1.

[13] S. Zhong, W. Wang, Y. Zhuang, Z. Huang, W. Shen, Adv. Funct. Mater. 2016, 26, 4768.

[14] K. Peng, J. Zhu, J. Electroanal. Chem. 2003, 558, 35.

[15] Y. Jiang, H. Shen, T. Pu, C. Zheng, Q. Tang, K. Gao, J. Wu, Ch. Rui, Y. Li, Y. Liu, Sol. Energy 2017, 142, 91.

[16] J. Wu, Y. Liu, W. Chen, Y. Zhao, Q. Chen, H. Tang, Y. Wang, X. Du, Appl. Surf. Sci. 2020, 506, 144778.

[17] A. Stapf, F. Honeit, C. Gondek, E. Kroke, Sol. Energy Mater. Sol. Cells 2017, 159, 112.

[18] K. Gao, Y. Liu, Y. Fan, L. Shi, Y. Zhuang, Y. Cui, S. Yuan, S. Wan, W. Shen, Z. Huang, Nanoscale Res. Lett. 2020, 15, 1.

[19] A. A. A. Omer, Z. He, S. Hong, Y. Chang, J. Yu, S. Li, W. Ma, W. Liu, W. E. Kolaly, R. Chen, Silicon 2021, 13, 351.

[20] C. Zhang, L. Chen, Y. Zhu, Z. Guan, Nanoscale Res. Lett. 2018, 13, 4.

[21] Y. Wang, L. Yang, Y. Liu, Z. Mei, W. Chen, J. Li, H. Liang, A. Kuznetsov, X. Du, Sci. Rep. 2015, 5, 1.

[22] P. Altermatt, O. Schumacher Jürgen, A. Cuevas, M. J. Kerr, S. W. Glunz, R. R. King, G. Heiser, A. Schenk, J. Appl. Phys. 2002, 92, 3187.

[23] H. Haug, A. Kimmerle, J. Greulich, A. Wolf, E. S. Marstein, Sol. Energy Mater. Sol. Cells 2014, 131, 30.

[24] H. Hauga, J. Greulichb, Energy Proc. 2016, 92, 60.

[25] A. A. Chowdhury, A. Ebong, 12th Int. Conf. on High-Capacity Optical Networks and Enabling/Emerging Technologies, HONET-ICT 2015, 2016, pp. 161–164.

[26] S. Sepeai, S. H. Zaidi, M. K. M. Desa, M.Y. Sulaiman, K. Sopian, J. Energy Technol. Policy 2013, 3, 1.

[27] X. Cai, X. Zhou, Z. Liu, F. Jiang, Q. Yu, Optik 2018, 164, 105.